Modeling CO and N_2 Adsorption at Cr Surface Species of Phillips Catalyst by Hybrid Density Functionals: Effect of Hartree−Fock Exchange Percentage†

Alessandro Damin,* Jenny G. Vitillo, Gabriele Ricchiardi, Silvia Bordiga, Carlo Lamberti, Elena Groppo, and Adriano Zecchina*

Dipartimento di Chimica IFM, and NIS (Nanostructured Interfaces and Surfaces) Centre of Excellence, University of Torino, Via P.Giuria 7, I-10125 Torino

Received: March 24, 2009; Revised Manuscript Received: June 29, 2009

In this article, we present a computational study of the structure and vibrational properties of the species formed by the interaction between Cr sites of Phillips catalyst and probe molecules (CO, N_2). The vibrational properties of these surface species, intensively investigated in the past, form a very rich and ideal set of experimental data to test computational approaches. By adopting the $X_4Si_2O_3Cr$ (X = H, OH, F) cluster as a simplified model of the $(\equiv SiO)_2Cr(II)$ species present at the surface of the real catalyst, we found that the B3LYP hybrid functional (containing 20% of Hartree−Fock exchange), when applied to this model, is unable to reproduce with reasonable accuracy the currently available experimental data (principally coming from IR spectroscopy). Better agreement is obtained when the percentage of Hartree−Fock exchange is increased (up to 35−40%).

1. Introduction

The Cr/SiO_2 Phillips catalyst is currently responsible for one-third of the polyethylene (PE) worldwide production.[1−3] Because of its industrial relevance, since its discovery it has attracted a great deal of academic and industrial research, being a subject of many investigations concerning the nature of the active sites and the exact initiation/polymerization mechanism.[1,3−8]

The catalyst is prepared by the esterification of surface sylanols (≡SiOH) pairs present on amorphous silica surface with H_2CrO_4 following the simple reaction

Step 1

$$2(\equiv SiOH) + H_2CrO_4 \rightarrow (\equiv SiO)_2CrO_2 + 2H_2O$$

leading to the formation of surface chromates. The surface chromates (formed at 923 K, that is, under conditions that lead to highly dehydroxilated silica) are then reduced by C_2H_4 or CO, with the formation of anchored Cr(II) species, following the general reaction[1,3]

Step 2

$$(\equiv SiO)_2CrO_2 + Red \rightarrow (\equiv SiO)_2Cr(II) + CH_2O/CO_2 \quad Red = C_2H_4 \text{ or CO}$$

Several species can be formed whose structure depends on the location of the parent silanols (vicinal, geminal, etc.). The widespread opinion[3,9,10] is that the surface chromate formed upon anchoring to vicinal silanols is by far the most abundant on the surface. (See the T model in Figure 1.) Less abundant structures formed by condensation with other silanols pairs (e.g., I and O models of Figure 1) can also be present in definitely smaller concentration.

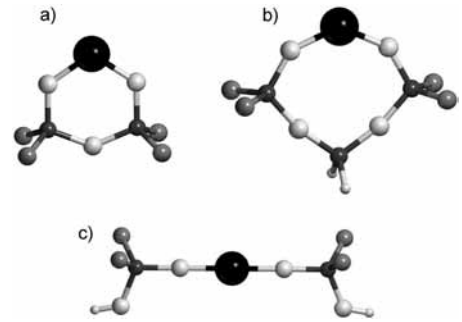

Figure 1. Graphical representation of the (a) T, (b) I, and (c) O models adopted in ref 29 to simulate the Cr(II) species of the Phillips catalyst: black spheres, Cr; dark gray spheres, Si; light gray spheres, F (in this study, F in T model is substituted by H or OH, too); big white spheres, O; small white spheres, H.

When reduction is performed by C_2H_4, the polymerization immediately starts, and the nature of active sites is consequently difficult to be investigated. Conversely, it is widely documented that if reduction is achieved by CO, then low-coordinated mononuclear Cr(II) grafted centers can be prepared, which are active in ethylene polymerization and have been characterized by means of several spectroscopic (UV−vis, IR, EXAFS, XANES, Raman)[3,11−18] and gravimetric techniques.[19]

Because there is general consensus that some of the Cr(II) sites, prepared following steps 1 and 2, are the active centers for ethylene polymerization,[1,3] it is evident that the Cr/SiO_2 system is representing one of the simplest examples of catalyst synthesized by means of an elementary and well-defined surface chemistry approach.

Despite the apparent structural simplicity, the precise definition of the active sites remains not fully clarified. This is mainly due to the disordered (amorphous) nature of the support, where different type of sylanol pairs are exposed on the surface (as discussed in ref 3) and where, consequently, similar families of chromates and grafted Cr(II) species can be formed. The families of coordinatively unsaturated Cr sites are characterized

† Part of the "Vincenzo Aquilanti Festschrift".

* Corresponding authors. (A.D.) E-mail: alessandro.damin@unito.it. Tel: +39-011-6707288. Fax: +39-011-6707855. (A.Z.) E-mail: adriano.zecchina@unito.it. Tel: +39-011-6707860. Fax: +39-011-6707855.

10.1021/jp902650m
Published on Web 07/17/2009

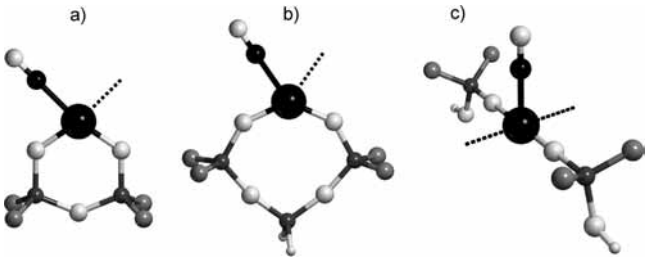

Figure 2. Graphical representation of the (a) T(CO), (b) I(CO), and (c) O(CO) models adopted in ref 29 to simulate the CO adsorption at Cr(II) species of the Phillips catalyst. Dashed lines show the position of the second CO molecule in T and I dicarbonyls and of the two CO molecules in O dicarbonyls: big black spheres, Cr; small black spheres, C; dark gray spheres, Si; light gray spheres, F (in this study, F in T model is substituted by H or OH too); big white spheres, O; small white spheres, H.

by the same oxidation state (divalent) but by a different coordination sphere: this is constituted by two chemically bonded oxygen atoms and by a variable number of additional weaker oxygen ligands, belonging to surface ≡Si−O−Si≡ siloxane groups in the adjacent position.

All of these highly coordinatively unsaturated Cr(II) sites readily adsorb O_2 (giving back the original chromates),[20] N_2,[14] CO,[3] and NO,[3] with formation of a variety of nitrogen, carbonylic, and nitrosylic complexes that have been fully characterized by spectroscopy techniques. In brief (a detailed description about this topic will be given in the following), when CO adsorption at RT is concerned, FTIR measurements show that $\tilde{\nu}_{CO}$ (stretching frequency) of the CO molecule interacting with surface species of Cr/SiO_2 is strongly perturbed, leading to the appearance of a complex envelope of bands (which is a function of the applied CO pressure) in the narrow 2170−2195 cm^{-1} range (i.e., substantially blue-shifted 37−47 cm^{-1} with respect to the $\tilde{\nu}_{CO}$ value of the free molecule).[3]

On the basis of the considerations previously discussed, the 2170−2195 cm^{-1} absorption is due to CO adsorbed on the most abundant species (the T species, see Figure 1).

Concerning the ethylene initiation/polymerization mechanism, many investigations have been carried out by using temperature-programmed FTIR experiments.[19,21−23] The following results have been firmly established: (i) upon C_2H_4 contact, Cr(II)/C_2H_4 complexes are initially formed on all surface sites; (ii) at RT, only a small fraction of exposed Cr(II) sites initiate a fast polymerization reaction, whereas the remaining ones behave as spectrators; and (iii) the initiation/polymerization reaction is so fast at RT that the initial intermediates can be observed only at low temperature in suitably designed temperature-programmed experiments. Despite these important achievements, the precise definition of the structure properties of the fraction of sites showing fast polymerization activity at RT is still missing.

Considering the abundant presence of experimental data and the unprecedented definition of many aspects of the surface structures, it is evident that computational methods could help in understanding in great detail how Cr(II) species interact with the silica support and toward ethylene molecules, giving some insight into the understanding of the initiation/polymerization process. In the last several years, only a few papers based on computational methods appeared about the simulation of Cr/SiO_2 catalyst, the most relevant ones coming from Espelid and Børve.[24−29] In these papers, three simple models of Cr/SiO_2 suface species were adopted, namely, T, I, and O. (See Figure 1.) Following refs 9 and 10, these three different structures were reasonably assumed to be representative of the multitude of sites that can be generated by reactions 1 and 2 on amorphous silica. However, because we know that the T species are by far the most concentrated, hereafter we notice that we will focus our attention on these species. Moreover, T-type species have also been currently considered for other silica-grafted metals (e.g., Mo and Ni).[30,31] In the adopted clusters, F atoms were used to saturate Si dangling bonds.[25−29] We shall see in the following that this assumption, based on the utilization of the very electronegative F atoms to saturate the dangling bonds, is more severe than the previous one and is representing one of the weak and debatable points of the models. When CO interaction with Cr(II) centers is considered,[26,29] it clearly emerges that the adopted computational scheme (calculations have been performed at the B3LYP level) is unable to reproduce the experimental data correctly, because it leads to strongly underestimated $\Delta\tilde{\nu}_{CO}$ ($\Delta\tilde{\nu}_{CO} = \tilde{\nu}_{CO}^{adduct} - \tilde{\nu}_{CO}^{free}$) with respect to the experimental values. Authors themselves recognize[26,29] that the B3LYP hybrid functional probably overestimates the charge transfer process, resulting in excessive back-donation from the metal centers to the π^* orbitals of the CO molecule, the final effect being too small computed or even negative $\Delta\tilde{\nu}_{CO}$.

Very recently, it has been clearly demonstrated by several authors that the ability of hybrid functionals (in particular, the B3LYP functional) to reproduce the experimental observables or quantities obtained at a higher level of theory can be improved by increasing the percentage of Hartree−Fock exchange.[32−35]

Stimulated by these new findings and after due consideration of the very accurate and reproducible set of experimental IR[3,6,18] and Raman[12,13] data of adsorbed CO, which can be used to test the validity of the computational approaches, we decided to adopt the same strategy in studying the CO adsorption at the Cr/SiO_2 surface species. In this article, we present, for the first time, results obtained by studying the effect of varying the percentage of Hartree−Fock exchange on the T model of Cr/SiO_2. Moreover, the present study is not restricted to F-terminated clusters as those of Espelide and Børve,[25−29] and other terminations (H, OH) are also considered that are compatible with the chemical species present on the surface. The final end is to study the vibrational properties of both mono- and dicarbonyls species formed on the Cr(II) T sites, to compare theoretical and experimental results, and to verify whether the use of appropriate hybrid functionals can correctly reproduce the experimental findings. Results concerning N_2 adsorption are also discussed and compared with the available experimental data.[14]

2. CO Interaction with Cr/SiO_2: A Brief Overview of Experimental and Modeling Results

The experimental data coming from IR and Raman spectroscopies and concerning the interaction of CO with Cr/SiO_2 form a very rich, well-established, and detailed set of data,[3,6,21] which can be used to check the validity of any computational approach concerning the structure and surface properties of grafted Cr(II) sites.

As is well known, CO interacts at RT with Cr(II) centers originating stable nonclassical carbonyls[36−38] characterized by well-defined IR bands in the 2200−2170 cm^{-1} region, whose intensity is a function of the CO pressure.[3,21] In the low regime of pressure, where the monocarbonylic species are favored, two peaks, centered, respectively, at 2180 and 2191 cm^{-1} (i.e., blue-shifted of +37 and +48 cm^{-1} with respect to the $\tilde{\nu}_{CO}$ of CO in the gas phase) are observed, which have been assigned to two monocarbonyls formed on two slightly different Cr(II) sites (named Cr_A and Cr_B, respectively)[21] differing for the coordina-

TABLE 1: Geometrical Features of C_{2v}-Optimized T_X (X = H, F, OH) Models with B3LYP, HFX*n* ($20 \le n \le 50$, $\Delta n = 10$), and BHHLYP Functionals[a]

model/symmetry	T_H/C_{2v}					
functional	B3LYP	HFX20	HFX30	HFX40	HFX50	BHHLYP
Cr−O	1.827	1.831	1.834	1.838	1.842	1.838
O−Cr−O	113.7	113.6	113.2	112.7	112.1	112.4
Si−O−Cr	124.2	124.2	124.4	124.5	124.7	124.6
Si−O	1.660	1.662	1.653	1.644	1.636	1.637
Cr APT charge	1.395	1.399	1.471	1.527	1.568	1.560
Cr MSD	3.997	3.998	4.003	4.004	4.002	3.993
model/symmetry	T_{OH}/C_{2v}					
functional	B3LYP	HFX20	HFX30	HFX40	HFX50	BHHLYP
Cr−O	1.829	1.834	1.837	1.840	1.843	1.840
O−Cr−O	112.4	112.3	111.7	111.1	110.5	110.6
Si−O−Cr	124.5	124.5	124.8	125.1	125.3	125.3
Si−O	1.635	1.637	1.628	1.619	1.612	1.612
Cr APT charge	1.444	1.447	1.512	1.561	1.596	1.589
Cr MSD	3.995	3.997	4.001	4.001	4.000	3.990
model/symmetry	T_F/C_{2v}					
functional	B3LYP	HFX20	HFX30	HFX40	HFX50	BHHLYP
Cr−O	1.838	1.843	1.846	1.849	1.852	1.849
O−Cr−O	110.3	110.3	109.6	108.9	108.3	108.4
Si−O−Cr	125.3	125.3	125.6	125.9	126.2	126.2
Si−O	1.627	1.628	1.619	1.611	1.603	1.604
Cr APT charge	1.463	1.465	1.523	1.567	1.600	1.593
Cr MSD	3.990	3.992	3.995	3.996	3.995	3.986

[a] Cr−O and Si−O distances are expressed in angstroms. O−Cr−O and Si−O−Cr angles in degrees. Cr APT charges and Cr MSD (Mulliken spin density) (|e|) are also listed.

tion sphere. The immense literature on the spectroscopy of metal carbonyls (both classical[39−41] and nonclassical)[36−38] shows that the stretching frequency of CO interacting with transition-metal ions is resulting from a delicate balance between a complex electrostatic effect (originating from the interaction between the electric field generated by the positively charged atom and the CO multipole moments and finally resulting in a blue shift of the CO stretching frequency),[42−45] polarization effect, and charge transfer (donation from 5σ orbital of CO to d orbitals of metal contributing to a blue shift of the $\tilde{\nu}_{CO}$, back-donation from d orbitals of metal to π^* orbitals of CO, the last determining a red-shift). On this basis, it is evident that the IR spectroscopy of adsorbed CO gives important information on the nature of the adsorbing Cr(II) species. In particular, the observed blue shifts testify that CO is interacting with positive centers and that back-donation from the metal is not able to compensate or overwhelm the polarization effect fully.

As the CO pressure is increased, the peak at 2180 cm^{-1} evolves into an intense doublet characterized by a peak at 2184 cm^{-1} and a shoulder at 2178 cm^{-1}, suggesting that the monocarbonyls at Cr_A sites are evolving into dicarbonyls. The two IR peaks can be assigned to the symmetric (hereafter $\tilde{\nu}_{CO}^{symm}$) and antisymmetric (hereafter $\tilde{\nu}_{CO}^{asymm}$) stretching modes of the two CO molecules.[21] Because the peak at 2191 cm^{-1} remains unaffected upon increasing the CO pressure, it is concluded that Cr_B sites are not able to give dicarbonyls (at least at RT). Notice that the baricenter of the 2178−2184 cm^{-1} doublet is still +38 cm^{-1} blue-shifted with respect to the CO gas. The ($\tilde{\nu}_{CO}^{asymm} - \tilde{\nu}_{CO}^{symm}$) difference (6 cm^{-1}) can be considered to be the experimental signature of the dicarbonylic structures: consequently, the comparison between this signature and the computational results is central to the scope of this article.

Modeling of Cr−carbonyl geometries and of the corresponding vibrational was investigated by Espelid and Børve[29] on the T, I, and O models. (See Figure 1.) The structural features and the computed $\Delta\tilde{\nu}_{CO}$ are briefly described in the following as the starting point of the present theoretical work. For the O model, the Si−Si distance has been fixed at 6.9 Å. Calculations have been performed on neutral F-terminated clusters by adopting the B3LYP hybrid functional in its unrestricted formalism. Spin multiplicity has been set to $2S + 1 = 5$ by assuming a 2+ valence on Cr and four unpaired electrons. In T- and I-type monocarbonyls, the CO molecule lies in the plane defined by the O−Cr−O atoms (Figure 2a,b); it is in the cis position with respect to one of the two oxygen atoms, and the whole structure has C_s symmetry. In T- and I-type dicarbonyls, the second CO molecule lies in the same plane, and it is in the *trans* position with respect to the other CO molecules (C_{2v} symmetry, see dashed lines in Figure 2a,b). In O-type monocarbonyls, the CO is still placed on the plane defined by O−Cr−O atoms, but it is in between the two oxygen atoms. (See Figure 2.) In O-type dicarbonyl, the CO molecules lie in the same plane of O−Cr−O atoms, but it is rotated 90° with respect to the monocarbonyl. (See the dashed lines in Figure 2c.) As far as the computed vibrational properties of mono- and dicarbonyls is concerned, the situation can be summarized as follows: (a) In T-type complexes, the computed $\Delta\tilde{\nu}_{CO}$ values are +7 cm^{-1} for monocarbonyl and +8 ($\tilde{\nu}_{CO}^{asymm}$) and +26 ($\tilde{\nu}_{CO}^{symm}$) for dicarbonyls (intensity ratio $I_{asymm}/I_{symm} = 1.2$). (b) Similar results are obtained for I-type species. (c) In O-type complexes, a blue shift of +15 for the monocarbonyl and +31 ($\tilde{\nu}_{CO}^{asymm}$) and +47 ($\tilde{\nu}_{CO}^{symm}$) for dicarbonyls (intensity ratio ∞, so $\tilde{\nu}_{CO}^{symm}$ peak should not be visible in IR spectrum) has been computed. On the basis of such results, Børve et al.[29] were forced to conclude that: (a) Because T-type carbonyls give too small $\Delta\tilde{\nu}_{CO}$ values with respect to the experimental values, the two peaks at 2191 and 2178 cm^{-1} observed in the low-pressure regime were necessarily assigned, respectively, to $\tilde{\nu}_{CO}^{symm}$ and $\tilde{\nu}_{CO}^{asymm}$ of dicarbonyls. (b) For the same reason, the peak at

2191 cm^{-1} was assigned to O-type dicarbonyls. (c) The peak at 2180 cm^{-1} was assigned (without reporting any computed $\Delta\tilde{\nu}_{CO}$) to a T-type monocarbonyl perturbed by the interaction with additional weak ligands such as ≡SiOH or siloxane groups. The situation does not change appreciably when dicarbonylic species are considered.

It is evident that computational results strongly disagree with the conclusions derived from experimental results, and, in particular, the computed $\Delta\tilde{\nu}_{CO}$ values for the various carbonylic species remain strongly underestimated. It is a matter of fact that the computed $\Delta\tilde{\nu}_{CO}$ values for T, I, and O monocarbonyls are in the +7 to +15 cm^{-1} interval, to be compared with the observed +37 and +48 cm^{-1} figures. This discrepancy is particularly relevant when considering that the F atoms, adopted to saturate Si dangling bonds of all models, are very electronegative species (probably more than ≡Si−O− groups present in silica); therefore, we expect the induction of a stronger localization of positive charges on Cr, so CO polarization and hence more positive $\Delta\tilde{\nu}_{CO}$ values are ultimately favored. In other words, the results of ref 29 show that even the strong effect of terminating the clusters with ad hoc electronegative atoms and the choice of extreme geometries are unable to bring the computed frequencies in accordance with the experiment. All of these considerations are suggesting that: (i) the computational scheme adopted in ref 29 is not able to describe properly the interaction occurring between CO molecule and the Cr species present at the Cr/SiO_2 surface; and (ii) a good starting point in solving this problem is to investigate, with criticism, how the B3LYP functional works on the models of silica proposed in ref 29 and eventually try to improve its performance by taking into account the recent findings reported, for example, in refs 32−34 and 46. This conviction is at the basis of the present investigation, which is devoted to the T-type complexes testing. In our opinion, the choice of only one type of structure does not limit the general validity of the testing procedure because the results reported in ref 29 on the T, I, and O models have clearly shown that the structure of the Cr sites influences the frequency of adsorbed CO only in a narrow interval.

3. Computational Details

All calculations have been performed with the Gaussian03 software package.[47] We have described C, N, O, F, Si, and Cr atoms by adopting the TZV basis set developed by Ahlrichs and coworkers.[48] Ahlrichs polarization functions have been added to Si and Cr. For C, N, O, and F atoms, polarization functions have been doubled, starting from the Ahlrichs standard functions and following an even-tempered recipe. We describe H atoms by adopting a standard 6-311++G(2d,2p) Pople basis set.[49,50]

The adopted model was the T model[29] (T_X, brutto formula $X_4Si_2O_3Cr$, X = H, OH, F). C_{2v} symmetry has been retained during the optimization of T_X and $T_X(CO)_2$; C_s symmetry has been imposed in the optimization of $T_X(CO)$ and $T_X(N_2)$ adducts.

Spin multiplicity has been fixed at 2S + 1 = 5, which corresponds to four unpaired electrons (as can be expected for Cr^{2+} species).[1,29] Spin contamination does not exceed the 0.3% of the expected S(S + 1) value for four unpaired electrons.

Energy convergence and thresholds for optimization have been set to the default values. A pruned (99 590) grid (keyword: INTEGRAL (grid = ultrafine)) has been adopted.

We have performed calculations by adopting standard B3LYP[51,52] (20% of Hartree−Fock exchange) and BHandHLYP[47,52] (hereafter BHHLYP, 50% of Hartree−Fock exchange) hybrid density functionals in their unrestricted formalism.

Moreover, by adopting the B[53] and LYP[52] exchange and correlation functionals, hybrid functionals (hereafter HFX*n*, *n* = 20, 30, 40, 50, see below) containing a different amount of Hartree−Fock exchange have been constructed according to the formula:

$$P_2E_X^{HF} + P_1(P_4E_X^{Slater} + P_3E_X^{nonlocal}) + P_6E_C^{local} + P_5E_C^{nonlocal}$$

where

$$P_2 = a_o = 0.2 \text{ to } 0.5, \quad \Delta = 0.1$$
$$P_1 = 1.0$$
$$P_4 = P_3 = a_X = 1 - a_0$$
$$P_6 = 1.0$$
$$P_5 = a_C = 1 - a_0$$

already applied in ref 32. P_2 (or a_0) establishes the amount of Hartree−Fock exchange adopted to define the functional. The bigger P_2 is, the higher is the amount of the adopted Hartree−Fock exchange. Therefore, we can define four different functionals, labeled as HFX*n*, where

$$n = 100P_2$$

Notice that HFX20 and HFX50 contain the same amount of Hartree−Fock exchange as B3LYP and BHHLYP, respectively.

Binding energies (BE, no BSSE correction) have been computed accordingly to the following formula[54]

$$BE(nCO) = E(T_X) + nE(CO) - E[T_X(CO)_n] \quad n = 1,2$$

$$BE(CO \rightarrow 2CO) = E[T_X(CO)] + E(CO) - E[T_X(CO)_2]$$

$$BE(N_2) = E(T_X) + E(N_2) - E[T_X(N_2)]$$

Test calculations to evaluate the BSSE (basis set superposition error) for the B3LYP functional and for one functional (HFX40) of the HFX*n* series have been performed on $T_X(CO)$ adducts (X = H, OH, F) and by adopting the counterpoise scheme, as implemented in the Gaussian03 code (keyword: COUNTERPOISE=2).

4. Results and Discussion

4.1. Naked T Sites. For all adopted functionals (B3LYP, BHHLYP, and HFX*n*), optimized neutral bare T_X (X = H, OH, F) models resulted in retaining the structure schematized in Figure 1a (see Table 1 for geometrical details) and a 2S + 1 = 5 spin multiplicity. This corresponds to four unpaired electrons that, from the analysis of the wave function, are localized on d-like orbitals of the Cr atom. In fact, the computed Mulliken spin density on Cr is quite near 4, as expected for Cr(II) species in high spin configuration. The LUMO (lowest unoccupied molecular orbital) resulted in being a d-like orbital on Cr, as schematized in Figure 3: all trials to fill this orbital resulted in less-stable structures (from an energetic point of view, see S1 paragraph of the Supporting Information for further details).

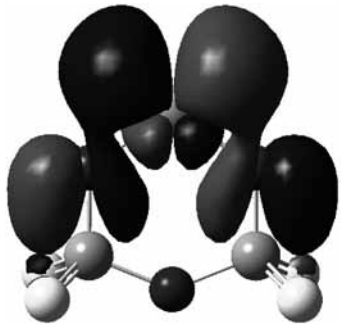

Figure 3. Graphical representation of the LUMO orbital obtained on the optimized T_F model: light gray spheres, Si and Cr; dark gray spheres, O; white spheres, F.

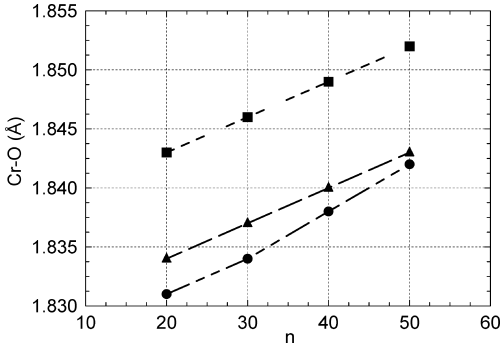

Figure 4. Cr−O distances (angstroms) as obtained along the whole series of HFXn ($20 < n < 50$, $\Delta n = 10$) functionals for the T_X optimized models: ●, X = H; ▲, X = OH; ■, X = F.

Table 1 and Figure 4 show that the obtained geometries (very close to those reported in ref 29) and the Cr APT charges[55] (the higher value being obtained for the F terminated clusters) are influenced by changing functionals and Si dangling bonds saturating groups. Conversely, Mulliken spin density on Cr is not affected by functional/Si dangling bonds. The analysis along the whole series of HFXn functionals shows that the Cr APT variation is an effect of the adopted amount of Hartree−Fock exchange. Finally, it has been noticed that HFX20 and HFX50 functionals give substantially the same results as B3LYP and BHHLYP, respectively.

4.2. Cr(CO) and Cr(CO)$_2$ Adducts. The results obtained on optimized monocarbonyl adducts (T_X(CO), C_s symmetry) are summarized in Table 2. The results obtained by employing the B3LYP functional for X = F are quite similar to those obtained in ref 29. It clearly appears that the B3LYP computed $\Delta\tilde{\nu}_{CO}$ is strongly affected upon changing the termination from X = F to X = H, OH, and it passes from positive to negative values. Only the more electronegative F terminations leads to the experimental positive sign of $\Delta\tilde{\nu}_{CO}$, the absolute value (+2 cm^{-1}) remaining, however, strongly underestimated when compared with the experimental figures (+37 to +48 cm^{-1}). The adoption of a more realistic T_X model, where X = $Si_6O_6H_{10}$ (i.e., the H, OH, and F terminal groups are substituted by siloxane moieties, as in silica; see Figure S4 in the S2 paragraph of the Supporting Information for a graphical representation), does not substantially change the situation because the computed $\Delta\tilde{\nu}_{CO}$ is still negative and very far from the experimental value (+6 cm^{-1} with respect to that obtained on the T_{OH} model). These findings seem to be in line with those obtained in studying the CO adsorption on Ni/MgO solid solution adopting the B3LYP functional[56] and seem to be related to the proper description of the exchange and correlation potentials in the presence of localized unpaired electrons, as is the case for Cr 3d states.[57] Conversely, the BHHLYP computed $\Delta\tilde{\nu}_{CO}$ values appear to be much higher than the corresponding experimental values, in particular, for X = F, and out of the experimental interval of +37 to +48 cm^{-1}. However, it is clear that, upon passing from the B3LYP to the BHHLYP functional (i.e., increasing the amount of Hartree−Fock exchange from 20 to 50%), the computed $\Delta\tilde{\nu}_{CO}$ values approach the experimental values, whichever X is considered. The changes in the computed $\Delta\tilde{\nu}_{CO}$ are accompanied by a change in the geometrical, electronic, and energetic properties. In particular, upon passing from the B3LYP to the BHHLYP functional, the Cr−C_{CO} distance is lengthened, the C−O distance is progressively shortened, CO MSD (Mulliken spin density) is reduced by about one order of magnitude, and BE is lowered by about 10 kJ mol^{-1}.

In conclusion, it clearly appears that whatever is the termination, the percentage of Hartree−Fock exchange adopted to define the hybrid density functional is strongly changing the type of interaction occurring between Cr in T model and the CO molecule, because overlap forces (in particular, the back-donation from metal to CO) contributing to the Cr···CO bond are gradually reduced. Lengthening of the Cr−C_{CO} distance, lowering in BE and CO MSD, and finally strong increase in $\Delta\tilde{\nu}_{CO}$ (documented in detail in Figure 5, where $\Delta\tilde{\nu}_{CO}$ vs n is reported) are simply the consequences of this modification. Further origin of higher and more positive $\Delta\tilde{\nu}_{CO}$ can be found in the corresponding increase in the electrostatic effect as a consequence of the increase in the higher amount of the Hartree−Fock exchange in the HFXn functionals. Finally, it has to be noticed that for $30 < n < 45$ (depending on X), the computed $\Delta\tilde{\nu}_{CO}$ values fall quite near to the experimental values.

BSSE (basis set superposition error) should not affect the observed trend because it results, from test calculations performed on T_X(CO) adducts (X = H, OH, F) with the B3LYP and the HFX40 functionals, to be very small (about 4% of the BE(CO); see Table 2 and the Computational Details section for further details).

When dicarbonyls adducts ($T_X(CO)_2$, C_{2v} symmetry) are concerned, the same conclusions can be drawn. (See the results reported in Table 3.) In fact, the increase in the percentage of Hartree−Fock exchange generally causes better agreement with experimental data, as it clearly appears from Figure 6, where $\Delta\tilde{\nu}_{CO}$ values computed (by HFXn functionals) on $T_{OH}(CO)_2$ and T_{OH}(CO) models are reported as a function of n. In particular, it can be noticed that upon increasing n from 20 to 50, $\Delta\tilde{\nu}_{CO}$ (as already observed for monocarbonyls) moves toward the experimental values, up to exceed them for $n = 50$. Moreover, the ($\tilde{\nu}_{CO}^{asymm} - \tilde{\nu}_{CO}^{symm}$) fingerprint difference associated with dynamic coupling of CO oscillators of the dicarbonylic structure (vertical line in Figure 6) also moved toward the experimental value as n increased ($n = 20$ gives a value of about 20 cm^{-1}, whereas a 6 cm^{-1} figure is computed for $n = 40$, which is very near the experimental value). Finally, for $30 < n < 40$, the relative position of $\tilde{\nu}_{CO}$ in monocarbonyl with respect to $\tilde{\nu}_{CO}^{asymm}$ and $\tilde{\nu}_{CO}^{symm}$ in dicarbonyl is ($\tilde{\nu}_{CO}^{asymm} < \tilde{\nu}_{CO} < \tilde{\nu}_{CO}^{symm}$) a fact that corresponds to the experimental observation. At this point, it is, however, worth mentioning that the calculated intensity ratio between $\tilde{\nu}_{CO}^{asymm}$ and $\tilde{\nu}_{CO}^{symm}$ is near 1.2 for all adopted functionals and X groups and that this figure does not agree with the experimental observation.[3,6,21]

From the above-described results and the comparison with experimental data, it clearly appears that the B3LYP functional is unable to describe the interaction between CO and Cr(II) species of Cr/SiO_2 correctly. On the contrary, the increase in the amount of Hartree−Fock exchange improves the quality of

TABLE 2: Selected Features of the Free CO Molecule and of the C_s-Optimized $T_X(CO)$ (X = H, F, OH) Adduct with B3LYP, HFX*n* ($20 \le n \le 50$, $\Delta n = 10$), and BHHLYP Functionals[a]

system	CO					
functional	B3LYP	HFX20	HFX30	HFX40	HFX50	BHHLYP
C−O	1.125	1.126	1.121	1.116	1.112	1.112
$\tilde{\nu}_{CO}$	2201	2195	2238	2278	2315	2313
model/symmetry	$T_H(CO)/C_S$					
functional	B3LYP	HFX20	HFX30	HFX40	HFX50	BHHLYP
<Cr−O>	1.845	1.850	1.856	1.861	1.864	1.861
O−Cr−O	106.0	106.1	106.7	107.2	107.4	107.5
Δ(C−O)	0.001	0.001	−0.003	−0.005	−0.007	−0.006
Cr−C_{CO}	2.105	2.119	2.169	2.214	2.253	2.230
CO MSD	0.097	0.092	0.040	0.011	−0.004	0.002
BE(CO)	+69.7(+66.6)	+64.2	+57.6	+54.2(+51.8)	+52.6	+59.0
$\Delta\tilde{\nu}_{CO}$	−31	−27	+10	+38	+57	+54
model/symmetry	$T_{OH}(CO)/C_S$					
functional	B3LYP	HFX20	HFX30	HFX40	HFX50	BHHLYP
<Cr−O>	1.847	1.852	1.858	1.862	1.866	1.862
O−Cr−O	105.1	105.2	105.7	105.9	106.1	106.1
Δ(C−O)	0.000	−0.001	−0.004	−0.006	−0.008	−0.007
Cr−C_{CO}	2.112	2.126	2.173	2.218	2.254	2.233
CO MSD	0.087	0.082	0.035	0.008	−0.005	0.001
BE(CO)	+72.3(+69.2)	+66.9	+60.8	+57.5(+55.1)	+55.9	62.2
$\Delta\tilde{\nu}_{CO}$	−20	−17	+17	+44	+63	+59
model/symmetry	$T_F(CO)/C_S$					
functional	B3LYP	HFX20	HFX30	HFX40	HFX50	BHHLYP
<Cr−O>	1.857	1.862	1.867	1.871	1.874	1.870
O−Cr−O	103.8	103.9	104.2	104.5	104.4	104.4
Δ(C−O)	−0.002	−0.003	−0.006	−0.007	−0.009	−0.008
Cr−C_{CO}	2.130	2.144	2.190	2.229	2.263	2.242
CO MSD	0.065	0.060	0.023	0.002	−0.008	−0.002
BE(CO)	+76.1(+73.2)	+70.9	+65.6	+62.7(+60.4)	+61.1	+67.3
$\Delta\tilde{\nu}_{CO}$	+2	+5	+36	+58	+74	+71

[a] C−O, <Cr−O>, Cr−C_{CO}, and Δ(C−O) [$(C-O)_{adduct} - (C-O)_{free}$] are expressed in angstroms. O−Cr−O angle in degrees. CO MSD (|e|): CO mulliken spin density. BE(CO): binding energy, kJ mol^{-1}; number in parentheses refers to the BSSE corrected values. $\Delta\tilde{\nu}_{CO}$ (cm^{-1}) = $\tilde{\nu}_{CO}^{adduct} - \tilde{\nu}_{CO}^{free}$.

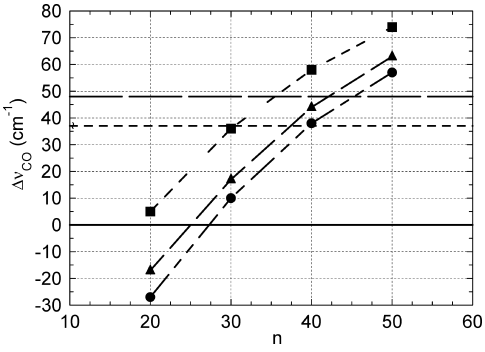

Figure 5. $\Delta\tilde{\nu}_{CO}$ (cm^{-1}) as computed along the whole series of HFX*n* ($20 \le n \le 50$, $\Delta n = 10$) functionals for the $T_X(CO)$ adducts: ●, X = H; ▲, X = OH; ■, X = F. For the sake of comparison, the experimental $\Delta\tilde{\nu}_{CO}$ values for Cr_A and Cr_B monocarbonyls are also reported (short and long dashed lines).

the results, the computed $\Delta\tilde{\nu}_{CO}$ value being in better agreement with the experimental values. However, from a closer inspection of Figure 5, we have to notice that the exact amount of Hartree−Fock exchange needed to reproduce the observed $\Delta\tilde{\nu}_{CO}$ cannot be established with full confidence. In fact, the optimum *n* value is also a function of which species is adopted to saturate Si dangling bonds. For the more electronegative terminations, the F groups, $n = 30$ is needed to match the experimental $\Delta\tilde{\nu}_{CO}$ (Cr_A monocarbonyls). When H or OH groups are employed, the optimum *n* moves toward higher values (40 or 37, respectively). The same holds when experimental $\Delta\tilde{\nu}_{CO}$ values for Cr_B are concerned. The optimum *n* values previously mentioned also give the best ($\tilde{\nu}_{CO}^{asymm} - \tilde{\nu}_{CO}^{symm}$) differences.

On the basis of these considerations, we have to expect that all parameters that could affect the electronic properties of Cr (i.e., the Cr−O distance and the O−Cr−O/Si−O−Cr angles) can change the optimum *n* value matching the experimental data. For this reason, although it is well established that functionals characterized by appropriately modulated HF exchange are definitely more appropriate in describing the surface chemistry of grafted Cr(II), we cannot use them to determine unambiguously whether the T model is the best candidate to simulate Cr_A/Cr_B species of the Phillips catalyst. It is evident that to answer this question fully, further investigations on other model structures with functionals characterized by modulated HF exchange are needed.

4.3. Cr(N_2) and Cr(N_2)$_2$ Adducts. To verify if, despite the above-described limitations, the previously discussed "Hartree−Fock recipe" can be fruitfully extended to the interaction of Cr(II) with other molecules, the interaction between Cr and N_2 molecules is studied and compared with experimental results. As clearly evidenced by IR[14] and Raman[13] spectroscopies, the N_2 molecule is able to give RT stable molecular adducts with

TABLE 3: Selected Features of the C_{2v}-Optimized $T_X(CO)_2$ (X = H, F, OH) Adducts with B3LYP, HFX*n* ($20 \le n \le 50$, $\Delta n = 10$), and BHHLYP Functionals[a]

model/symmetry	$T_H(CO)_2/C_{2v}$					
functional	B3LYP	HFX20	HFX30	HFX40	HFX50	BHHLYP
Cr−O	1.875	1.880	1.884	1.888	1.889	1.887
O−Cr−O	99.7	99.8	101.0	101.8	102.5	102.4
Δ(C−O)	−0.001	−0.001	−0.004	−0.005	−0.006	−0.005
Cr−C_{CO}	2.140	2.157	2.198	2.237	2.269	2.245
CO MSD	0.048	0.044	0.016	0.000	−0.008	−0.003
BE(2CO)	+125.5	+114.3	+105.1	+100.2	+97.8	+111.3
BE(CO→2CO)	+55.9	+50.1	+47.5	+46.0	+45.1	+52.4
$\Delta\tilde{\nu}_{CO}^{asymm}$	−23	−19	+11	+34	+50	+47
$\Delta\tilde{\nu}_{CO}^{symm}$	0	+2	+25	+43	+55	+53
model/symmetry	$T_{OH}(CO)_2/C_{2v}$					
functional	B3LYP	HFX20	HFX30	HFX40	HFX50	BHHLYP
Cr−O	1.875	1.880	1.885	1.888	1.890	1.887
O−Cr−O	99.1	99.2	100.2	101.0	101.5	101.4
Δ(C−O)	−0.002	−0.002	−0.004	−0.006	−0.007	−0.006
Cr−C_{CO}	2.144	2.161	2.202	2.240	2.271	2.247
CO MSD	0.045	0.040	0.014	−0.001	−0.009	−0.003
BE	+131.5	+120.4	+111.6	+106.6	+104.1	+117.6
BE(CO→2CO)	+59.2	+53.5	+50.8	+49.2	+48.2	+55.4
$\Delta\tilde{\nu}_{CO}^{asymm}$	−14	−10	+19	+40	+55	+52
$\Delta\tilde{\nu}_{CO}^{symm}$	+7	+10	+32	+48	+60	+57
model/symmetry	$T_F(CO)_2/C_{2v}$					
functional	B3LYP	HFX20	HFX30	HFX40	HFX50	BHHLYP
Cr−O	1.886	1.890	1.894	1.896	1.898	1.895
O−Cr−O	98.4	98.5	99.3	99.8	100.2	100.2
Δ(C−O)	−0.003	−0.004	−0.006	−0.007	−0.008	−0.007
Cr−C_{CO}	2.154	2.170	2.210	2.246	2.275	2.252
CO MSD	0.035	0.031	0.008	−0.004	−0.011	−0.005
BE	+139.7	+128.8	+120.7	+116.0	+113.4	+126.7
BE(CO→2CO)	+63.6	+57.9	+55.1	+53.4	+52.3	+59.4
$\Delta\tilde{\nu}_{CO}^{asymm}$	+4	+8	+34	+53	+65	+63
$\Delta\tilde{\nu}_{CO}^{symm}$	+22	+25	+45	+60	+70	+68

[a] C−O, Cr−O, Cr−C_{CO}, and Δ(C−O) [$(C-O)_{adduct} - (C-O)_{free}$] are expressed in angstroms. O−Cr−O angle in degrees. CO MSD (|e|): CO Mulliken spin density. BE(CO) and BE(CO→2CO): binding energies, kJ mol^{-1}. $\Delta\tilde{\nu}_{CO}^{asymm} = \tilde{\nu}_{CO}^{asymm}(adduct) - \tilde{\nu}_{CO}(free)$ and $\Delta\tilde{\nu}_{CO}^{symm} = \tilde{\nu}_{CO}^{symm}(adduct) - \tilde{\nu}_{CO}(free)$ are expressed in cm^{-1}.

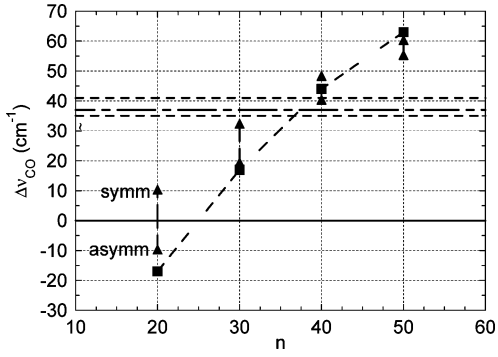

Figure 6. $\Delta\tilde{\nu}_{CO}^{asymm}$ and $\Delta\tilde{\nu}_{CO}^{symm}$ (inverse centimeters) as computed along the whole series of HFX*n* ($20 \le n \le 50$, $\Delta n = 10$) functionals for the $T_{OH}(CO)_2$ adduct (▲). For the sake of comparison, the computed $\Delta\tilde{\nu}_{CO}$ (cm^{-1}, ■) values for the $T_{OH}(CO)$ adduct and the experimental values for Cr_A monocarbonyls (dashed and dotted line) and Cr_A dicarbonyls (dashed lines) are also reported.

Cr(II) species of Cr/SiO_2 system. A narrow band at 2328 cm^{-1} ($\Delta\tilde{\nu}_{NN} = -3$ cm^{-1} with respect to $\tilde{\nu}_{NN}$ of the free N_2 molecule) and a weaker component at 2337 cm^{-1} ($\Delta\tilde{\nu}_{NN} = +6$ cm^{-1}) are observed and assigned to $Cr_A\cdots N_2$ and $Cr_B\cdots N_2$ monoadducts, respectively. When the temperature is lowered to 77 K, Cr_A sites coordinate a second N_2 molecule, as demonstrated by the fact that the peak at 2328 cm^{-1} moves to 2333 cm^{-1}; conversely, Cr_B species are not able to coordinate a second N_2 molecule because the peak located at 2337 cm^{-1} remains unaffected.

As for the Cr(II)/CO interaction, T_X (X = H, OH, F) models have been employed to study the formation of N_2 monoadducts at Cr(II) sites of Cr/SiO_2. Results are summarized in Table 4 and Figure 7. It is immediately evident that the B3LYP functional is unable to reproduce the experimental $\Delta\tilde{\nu}_{NN}$ correctly, leading to a red shift that is too high (−42 cm^{-1} for the $T_F(N_2)$ adduct). As already observed for T_X carbonyls, the increase in the amount of exact Hartree−Fock exchange adopted to define the hybrid functional corrects toward the experimental data. (See Figure 7, where $\Delta\tilde{\nu}_{NN}$ is plotted vs *n*.) This result is parallel to that obtained for the Cr(II)/CO interaction and clearly shows that the adopted strategy is basically correct and characterized by general validity.

Finally, the comparison between data reported in Figure 4 ($\Delta\tilde{\nu}_{CO}$ vs *n*) and Figure 7 ($\Delta\tilde{\nu}_{NN}$ vs *n*) shows that the *n* value needed to match the experimental $\Delta\tilde{\nu}_{CO}$ value for Cr_A monocarbonyls[21] and that the experimental data concerning N_2 adducts[14] are different ($n_{CO} = 37$ vs $n_{N2} = 35$ when X = OH is concerned; solid triangles in Figures 5 and 7, respectively). The effect, although not very dramatic, suggests that care must be taken in extending the *n* value determined for a type of interaction (i.e., for Cr···CO adducts) to another one (i.e., $Cr\cdots N_2$ adducts).

TABLE 4: Selected Features of the Free N_2 Molecule and of the C_s-Optimized $T_X(N_2)$ (X = H, F, OH) Adduct with B3LYP, HFX*n* ($20 \le n \le 50$, $\Delta n = 10$), and BHHLYP Functionals[a]

system	N_2					
functional	B3LYP	HFX20	HFX30	HFX40	HFX50	BHHLYP
N−N	1.091	1.091	1.086	1.081	1.076	1.077
$\tilde{\nu}_{NN}$	2444	2439	2491	2541	2588	2582
model/symmetry	$T_H(N_2)/C_S$					
functional	B3LYP	HFX20	HFX30	HFX40	HFX50	BHHLYP
<Cr−O>	1.845	1.850	1.854	1.857	1.860	1.857
O−Cr−O	107.1	107.2	107.9	108.1	108.2	108.1
Δ(N−N)	0.003	0.003	0.000	−0.001	−0.002	−0.002
$Cr-N_{N2}$	2.135	2.156	2.218	2.260	2.290	2.255
N_2 MSD	0.054	0.046	0.010	−0.004	−0.001	−0.006
$BE(N_2)$	+35.9	+31.5	+28.9	+28.5	+29.1	+34.6
$\Delta\tilde{\nu}_{NN}$	−69	−63	−18	+3	+15	+13
model/symmetry	$T_{OH}(N_2)/C_S$					
functional	B3LYP	HFX20	HFX30	HFX40	HFX50	BHHLYP
<Cr−O>	1.846	1.852	1.856	1.859	1.861	1.858
O−Cr−O	106.2	106.3	106.6	106.8	106.8	106.7
Δ(N−N)	0.002	0.002	−0.001	−0.002	−0.002	−0.002
$Cr-N_{N2}$	2.139	2.160	2.216	2.257	2.283	2.249
N_2 MSD	0.047	0.040	0.008	−0.005	−0.001	−0.006
$BE(N_2)$	+38.9	+34.6	+32.2	+31.8	+32.1	+37.8
$\Delta\tilde{\nu}_{NN}$	−61	−54	−13	+6	+16	+15
model/symmetry	$T_F(N_2)/C_S$					
functional	B3LYP	HFX20	HFX30	HFX40	HFX50	BHHLYP
<Cr−O>	1.856	1.861	1.865	1.867	1.870	1.866
O−Cr−O	104.7	104.8	105.0	105.1	105.0	105.0
Δ(N−N)	0.001	0.001	−0.001	−0.002	−0.002	−0.002
$Cr-N_{N2}$	2.151	2.172	2.220	2.251	2.273	2.243
N_2 MSD	0.033	0.027	0.003	−0.007	−0.010	−0.006
$BE(N_2)$	+44	+39.7	+37.8	+37.4	+37.6	+43.3
$\Delta\tilde{\nu}_{NN}$	−42	−37	−6	+10	+18	+17

[a] N−N, <Cr−O>, $Cr-N_{N2}$, and Δ(N−N) [$(N-N)_{adduct} - (N-N)_{free}$] are expressed in angstroms. O−Cr−O angle in degrees. N_2 MSD (|e|): N_2 Mulliken spin density. $BE(N_2)$: binding energy, kJ mol^{-1}. $\Delta\tilde{\nu}_{NN}$ (cm^{-1}) = $\tilde{\nu}_{NN}^{adduct} - \tilde{\nu}_{NN}^{free}$.

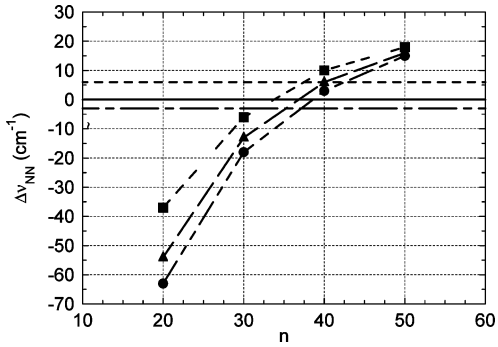

Figure 7. $\Delta\tilde{\nu}_{NN}$ (cm^{-1}) as computed along the whole series of HFX*n* ($20 \le n \le 50$, $\Delta n = 10$) functionals for the $T_X(N_2)$ adducts: ●, X = H; ▲, X = OH; ■, X = F. For the sake of comparison, the experimental $\Delta\tilde{\nu}_{NN}$ values are also reported (short and long dashed lines).

5. Conclusions

In this article, we presented a computational study on the interaction between surface Cr(II) species of Phillips catalyst and probe molecules (CO, N_2) that in the past have been widely employed for their characterization. By adopting the T_X (X = H, OH, F; see Figure 1 for a graphical representation of T_F) cluster as a simplified model of the $(\equiv SiO)_2Cr(II)$ species possibly present at the surface of the real catalyst, we found that the B3LYP hybrid functional (containing 20% of Hartree−Fock exchange) is unable to reproduce with reasonable accuracy the experimental data (mainly coming from IR spectroscopy) that are currently available. Better agreement is obtained when the percentage of Hartree−Fock exchange is increased (up to 35−40%). However, we cannot precisely define the exact amount of Hartree−Fock exchange (nor the error of such an approach), and further investigations, in particular, by adopting different models (characterized by different Cr−O distances and O−Cr−O/Si−O−Cr angles) of the $(\equiv SiO)_2Cr(II)$ are needed. The work has to be considered to be a necessary and important preliminary study of the modeling of Cr(II) interaction with ethylene molecule, that is, the monomer of the polymerization reaction.

Acknowledgment. Prof. P. Ugliengo (Dipartimento di Chimica IFM, Università di Torino) is acknowledged for fruitful and capital discussions. NIS Centre of Excellence of Università di Torino is also acknowledged for funding.

Supporting Information Available: Analysis of the wave function on T_F model and structure of the CO adduct on the T model derived from silicalite as obtained at the B3LYP level. This material is available free of charge via the Internet at http://pubs.acs.org.

References and Notes

(1) McDaniel, M. P. *Adv. Catal.* **1985**, *33*, 47–98.

(2) Weckhuysen, B. M.; Schoonheydt, R. A. *Catal. Today* **1999**, *51*, 215–221.
(3) Groppo, E.; Lamberti, C.; Bordiga, S.; Spoto, G.; Zecchina, A. *Chem. Rev.* **2005**, *105*, 115–183, and references therein.
(4) Zecchina, A.; Garrone, E.; Ghiotti, G.; Morterra, C.; Borello, E. *J. Phys. Chem.* **1975**, *79*, 966–972.
(5) Zecchina, A.; Garrone, E.; Morterra, C.; Coluccia, S. *J. Phys. Chem.* **1975**, *79*, 978–983.
(6) Zecchina, A.; Garrone, E.; Ghiotti, G.; Coluccia, S. *J. Phys. Chem.* **1975**, *79*, 972–978.
(7) Ghiotti, G.; Garrone, E.; Zecchina, A. *J. Mol. Catal.* **1988**, *46*, 61–77.
(8) Weckhuysen, B. M.; Wachs, I. E.; Shoonheydt, R. A. *Chem. Rev.* **1996**, *96*, 3327–3349.
(9) Deslauriers, P. J.; McDaniel, M. P. *J. Polym. Sci., Part A: Polym. Chem.* **2007**, *45*, 3135–3149.
(10) McDaniel, M. P.; Collins, K. S.; Benham, E. A.; Cymbaluk, T. H. *Appl. Catal., A* **2008**, *335*, 252–261.
(11) Groppo, E.; Prestipino, C.; Cesano, F.; Bonino, F.; Bordiga, S.; Lamberti, C.; Thüne, P. C.; Niemantsverdriet, J. W.; Zecchina, A. *J. Catal.* **2005**, *230*, 98–108.
(12) Damin, A.; Bonino, F.; Bordiga, S.; Groppo, E.; Lamberti, C.; Zecchina, A. *ChemPhysChem.* **2006**, *7*, 342–344.
(13) Groppo, E.; Damin, A.; Bonino, F.; Zecchina, A.; Bordiga, S.; Lamberti, C. *Chem. Mater.* **2005**, *17*, 2019–2027.
(14) Groppo, E.; Lamberti, C.; Bordiga, S.; Spoto, G.; Zecchina, A. *J. Phys. Chem. B* **2005**, *109*, 15024–15031.
(15) Weckhuysen, B. M.; Deridder, L. M.; Schoonheydt, R. A. *J. Phys. Chem.* **1993**, *97*, 4756–4763.
(16) Weckhuysen, B. M.; Schoonheydt, R. A.; Jehng, J. M.; Wachs, I. E.; Cho, S. J.; Ryoo, R.; Kijlstra, S.; Poels, E. *J. Chem. Soc., Faraday Trans.* **1995**, *91*, 3245–3253.
(17) Weckhuysen, B. M.; Wachs, I. E. *J. Phys. Chem.* **1996**, *100*, 14437–14442.
(18) Rebenstorf, B.; Larsson, R. *J. Mol. Catal.* **1981**, *11*, 247–256.
(19) Groppo, E.; Lamberti, C.; Spoto, G.; Bordiga, S.; Magnacca, G.; Zecchina, A. *J. Catal.* **2005**, *236*, 233–244.
(20) Fubini, B.; Ghiotti, G.; Stradella, L.; Garrone, E.; Morterra, C. *J. Catal.* **1980**, *66*, 200–213.
(21) Zecchina, A.; Spoto, G.; Ghiotti, G.; Garrone, E. *J. Mol. Catal.* **1994**, *86*, 423–446.
(22) Groppo, E.; Lamberti, C.; Bordiga, S.; Spoto, G.; Zecchina, A. *J. Catal.* **2006**, *240*, 172–181.
(23) Lamberti, C.; Groppo, E.; Spoto, G.; Bordiga, S.; Zecchina, A. *Adv. Catal.* **2007**, *51*, 1–74.
(24) Espelid, Ø.; Børve, K. J. *J. Catal.* **2000**, *195*, 125–139.
(25) Espelid, Ø.; Børve, K. J. *Catal. Lett.* **2001**, *75*, 49–54.
(26) Espelid, Ø. Theoretical Models of Active Sites at Cr/Silica Phillips-Type Catalysts for Ethylene Polymerization. Ph.D. Thesis in Chemistry, Bergen, Norway, 2001.
(27) Espelid, Ø.; Børve, K. J. *J. Catal.* **2002**, *206*, 331–338.
(28) Espelid, Ø.; Børve, K. J. *J. Catal.* **2002**, *205*, 366–374.
(29) Espelid, Ø.; Børve, K. J. *J. Catal.* **2002**, *205*, 177–190.
(30) Costa, D.; Martra, G.; Che, M.; Manceron, L.; Kermarec, M. *J. Am. Chem. Soc.* **2002**, *124*, 7210–7217.
(31) Lopez, N.; Illas, F.; Pacchioni, G. *J. Mol. Catal. A: Chem.* **2001**, *170*, 175–186.
(32) Poater, J.; Sola, M.; Rimola, A.; Rodriguez-Santiago, L.; Sodupe, M. *J. Phys. Chem. A* **2004**, *108*, 6072–6078.
(33) Corà, F.; Alfredsson, M.; Mallia, G.; Middlemiss, D. S.; Mackrodt, W. C.; Dovesi, R.; Orlando, R. The Performance of Hybrid Density Functionals in Solid State Chemistry. In *Principles and Applications of Density Functional Theory in Inorganic Chemistry II*; Springer: Berlin, 2004; Vol. 113; pp 171−232.
(34) Corà, F. *Mol. Phys.* **2005**, *103*, 2483–2496.
(35) Valero, R.; Gomes, J. R. B.; Truhlar, D. G.; Illas, F. *J. Chem. Phys.* **2008**, *129*, 124710.
(36) Lupinetti, A. J.; Frenking, G.; Strauss, S. H. *Angew. Chem., Int. Ed.* **1998**, *37*, 2113–2116.
(37) Lupinetti, A. J.; Strauss, S. H.; Frenking, G. Nonclassical Metal Carbonyls In *Progress in Inorganic Chemistry*, 2001; Vol. 49, pp. 1−112.
(38) Strauss, S. H. *J. Chem. Soc., Dalton Trans.* **2000**, 1–6.
(39) Manoilova, O. V.; Penarroya Mentruit, M.; Tunes Palomino, G.; Tsyganenko, A. A.; Otero Areán, C. *Vibr. Spectr.* **2001**, *26*, 107–111.
(40) Otero Areán, C.; Tsyganenko, A. A.; Escalona Platero, E.; Garrone, E.; Zecchina, A. *Angew. Chem.* **1998**, *37*, 3161–3163.
(41) Otero Areán, C.; Manoilova, O. V.; Rodríguez Delgado, M.; Tsyganenko, A. A.; Garrone, E. *Phys. Chem. Chem. Phys.* **2001**, *3*, 4187–4188.
(42) Lamberti, C.; Bordiga, S.; Geobaldo, F.; Zecchina, A.; Arean, C. O. *J. Chem. Phys.* **1995**, *103*, 3158–3165.
(43) Pacchioni, G.; Cogliandro, G.; Bagus, P. S. *Int. J. Quant. Chem.* **1992**, *42*, 1115–1139.
(44) Damin, A.; Dovesi, R.; Zecchina, A.; Ugliengo, P. *Surf. Sci.* **2001**, *479*, 255–272.
(45) Ferrari, A. M.; Ugliengo, P.; Garrone, E. *J. Chem. Phys.* **1996**, *105*, 4129–4139.
(46) Grau-Crespo, R.; Corà, F.; Sokol, A. A.; de Leeuw, N. H.; Catlow, C. R. A. *Phys. Rev. B* **2006**, *73*, 035116.
(47) Frisch, M. J.; Trucks, G. W.; Schlegel, H. B.; Scuseria, G. E.; Robb, M. A.; Cheeseman, J. R.; Montgomery, J. A., Jr.; Vreven, T.; Kudin, K. N.; Burant, J. C.; Millam, J. M.; Iyengar, S. S.; Tomasi, J.; Barone, V.; Mennucci, B.; Cossi, M.; Scalmani, G.; Rega, N.; Petersson, G. A.; Nakatsuji, H.; Hada, M.; Ehara, M.; Toyota, K.; Fukuda, R.; Hasegawa, J.; Ishida, M.; Nakajima, T.; Honda, Y.; Kitao, O.; Nakai, H.; Klene, M.; Li, X.; Knox, J. E.; Hratchian, H. P.; Cross, J. B.; Bakken, V.; Adamo, C.; Jaramillo, J.; Gomperts, R.; Stratmann, R. E.; Yazyev, O.; Austin, A. J.; Cammi, R.; Pomelli, C.; Ochterski, J. W.; Ayala, P. Y.; Morokuma, K.; Voth, G. A.; Salvador, P.; Dannenberg, J. J.; Zakrzewski, V. G.; Dapprich, S.; Daniels, A. D.; Strain, M. C.; Farkas, O.; Malick, D. K.; Rabuck, A. D.; Raghavachari, K.; Foresman, J. B.; Ortiz, J. V.; Cui, Q.; Baboul, A. G.; Clifford, S.; Cioslowski, J.; Stefanov, B. B.; Liu, G.; Liashenko, A.; Piskorz, P.; Komaromi, I.; Martin, R. L.; Fox, D. J.; Keith, T.; Al-Laham, M. A.; Peng, C. Y.; Nanayakkara, A.; Challacombe, M.; Gill, P. M. W.; Johnson, B.; Chen, W.; Wong, M. W.; Gonzalez, C.; Pople, J. A. *Gaussian 03*, revision B.05; Gaussian, Inc.: Wallingford, CT, 2004.
(48) Schäfer, A.; Huber, C.; Ahlrichs, R. *J. Chem. Phys.* **1994**, *100*, 5829–5835.
(49) Clark, T.; Chandrasekhar, J.; Spitznagel, G. W.; Schleyer, P. v. R. *J. Comput. Chem.* **1983**, *4*, 294.
(50) Frisch, M. J.; Pople, J. A.; Binkley, J. S. *J. Chem. Phys.* **1984**, *80*, 3265–3269.
(51) Becke, A. D. *J. Chem. Phys.* **1993**, *98*, 5648–5652.
(52) Lee, C.; Yang, W.; Parr, R. G. *Phys. Rev. B* **1988**, *37*, 785–789.
(53) Becke, A. D. *Phys. Rev. A* **1988**, *38*, 3098–3100.
(54) Lendvay, G.; Mayer, I. *Chem. Phys. Lett.* **1998**, *297*, 365–373.
(55) Cioslowski, J. *J. Am. Chem. Soc.* **1989**, *111*, 8333–8336.
(56) Pacchioni, G.; Di Valentin, C.; Dominguez-Ariza, D.; Illas, F.; Bredow, T.; Kluner, T.; Staemmler, V. *J. Phys. Condens. Matter* **2004**, *16*, S2497−S2507.
(57) Martin, R. L.; Illas, F. *Phys. Rev. Lett.* **1997**, *79*, 1539–1542.

JP902650M